JOURNAL OF THERMOPHYSICS AND HEAT TRANSFER
Vol. 9, No. 2, April–June 1995

Investigation of the Freezing Blowby Phenomenon in Heat Pipes

J. M. Ochterbeck* and G. P. Peterson†
Texas A&M University, College Station, Texas 77843

The freezing blowby phenomenon in operating heat pipes has been previously hypothesized and experimentally induced under laboratory conditions, however, no naturally occurring 1-*g* experimental evidence has been presented to explain possible causes and results of this phenomenon. For this reason, an experimental investigation designed to evaluate and better define the overall characteristics of freezing blowby was conducted using a copper/water heat pipe for which freezing blowby conditions were found to occur naturally. Visual observations of the freezing blowby phenomenon were made, along with internal temperature and pressure measurements. The results from various rates of restart heat addition and channel blockage indicate that upon breakthrough, the depressurization of the evaporator results in an effective heat transport capacity in excess of the steady-state transport limit. The effective transport capacity was determined to easily exceed the capillary pumping capability of the heat pipe by an order of magnitude. The resulting transient conditions can cause a loss of liquid in the evaporator and potential dryout. Evidence is presented indicating that in order to prevent either temporary or permanent dryout, sufficient liquid inventory must be present in the evaporator wicking structure to accommodate the increased transient thermal load.

Nomenclature

A = area
c = specific heat
dA = differential area
f = friction factor
h = heat transfer coefficient
j = mass flux per unit area per unit time
L = length
l = length (time dependent)
M = molecular mass
m = mass
P = pressure, power
q = heat transfer rate
R = universal gas constant
Re = Reynolds number
r = radius
T = temperature
t = time
V = volume
α = accommodation coefficient
ε = porosity
λ = latent heat of vaporization
μ = viscosity
ρ = density
σ = surface tension

Subscripts
a = adiabatic
b = blockage, breakthrough
c = condenser, capillary
e = evaporator
eff = effective
g = gas front
h = hydraulic
l = liquid
m = melt front
s = saturation
v = vapor

Presented as Paper 92-2909 at the AIAA 27th Thermophysics Conference, Nashville, TN, July 6–8, 1992; received Oct. 13, 1993; revision received June 1, 1994; accepted for publication Sept. 27, 1994.

*Currently Assistant Professor of Mechanical Engineering, Clemson University, Clemson, SC 29634. Member AIAA.

†Head and Tenneco Professor, Department of Mechanical Engineering. Associate Fellow AIAA.

Introduction

FREEZING blowby describes the phenomenon occurring when a complete solid blockage, formed by freezing of the working fluid, of the vapor and liquid passages in a heat pipe is melted. This blockage of the channels effectively decouples the evaporator from the condenser such that during the process of melting, a pressure differential exists between the high-pressure evaporator region and the low-pressure condenser region. When dissipation of the blockage has progressed sufficiently to allow for breakthrough of the blockage, liquid may be driven from the high-pressure evaporator region into the lower pressure condenser region where subfreezing temperatures may or may not exist. If enough liquid is transported into the condenser region, depletion of liquid in the evaporator wicking structure and dryout can result.

The occurrence of freezing blowby was first postulated by Antoniuk and Edwards during the evaluation of several anomalous deprimings in the variable conductance heat pipes (VCHPs) utilized in the thermal management system of the Communication Technology Satellite (CTS).[1,2] The initial hypothesized failure modes included 1) generation of gas bubbles in the liquid arteries, 2) mechanical accelerations, 3) exceeding heat pipe capacity, and 4) liquid inventory depletions, of which freezing blowby was a subset. To allow for proper priming in 1-*g* testing, the VCHPs of interest were overcharged; however, in a 0-*g* environment, this excess charge bridged the vapor passage in the condenser.[1] In situations where the environmental sink temperature, and correspondingly, portions of the condenser region fall below the freezing point of the working fluid, this bridge could freeze and form a solid blockage of the vapor and liquid channels.

Further experimental[1,2] and analytical[1,3] investigations demonstrated that freezing blowby was a possible depriming mechanism, however, it was determined that this mechanism most probably did not cause the anomalous failures onboard the CTS. To verify the freezing blowby phenomena in ground

experiments, localized freezing in the condenser region was required to induce the solid blockage formation since the liquid bridge in the condenser was not a naturally occurring phenomena in a 1-*g* environment. In the analytical modeling of the solid barrier, the frozen solid blockage was assumed to be of negligible thickness and to thaw only when the environmental sink temperature was elevated above the triple point of the working fluid. The effects of the blockage magnitude and the effects of variations in evaporator heat input rate required to melt the blockage were not evaluated.

A more recent investigation into the freeze/thaw characteristics of a copper/water heat pipe, with varying levels of noncondensible gases (NCG), resulted in experimental observation, both visual and thermal, of the formation of a vapor and liquid channel solid blockage during the freezing process in a 1-*g* environment.[4] This was the first time that solid blockage of the vapor channel was observed to form naturally in a heat pipe operating in a 1-*g* environment. In this investigation, after heat was discontinued to the evaporator, the formation of the blockage required several hours and was found to occur at or near the diffusion zone located at the gas/vapor front. For the heat pipe tested, three distinctive regions were found to exist as a direct function of the noncondensible gas charge present in the heat pipe: 1) solid blockage formation along with evaporator dryout at low levels of NCG, 2) no blockage formation and a fully primed evaporator at high levels of NCG, and 3) solid blockage formation and a primed evaporator with intermediate levels of NCG.

For levels of NCG that resulted in a primed evaporator and a solid blockage formation (case 3), the freezing blowby phenomenon was visually observed as the blockage was melted. However, depriming of the evaporator for this case was not experienced during restart, as low evaporator heat addition rates were used, thereby resulting in a low-pressure differential and low levels of liquid blowby upon breakthrough of the solid blockage. While this investigation provided definitive evidence that freezing blowby could occur in a 1-*g* test pipe, quantitative evidence remained unavailable.

Experimental Investigation

To better understand the freezing blowby phenomenon and provide quantitative pressure and temperature data, an experimental investigation designed to evaluate and define the overall characteristics of freezing blowby in a copper/water heat pipe was conducted. This investigation included visual observations of the freezing blowby phenomenon along with temperature and pressure measurements for varying rates of heat addition, and thus, different pressure differentials across the blockage.

Experimental Apparatus

The experimental apparatus utilized in this investigation consisted of a copper/water heat pipe with an overall length of 2.0 m and internal dimensions of 25.4 by 11 mm, as illustrated in Fig. 1, and has been previously described in detail by Ochterbeck and Peterson.[4] A small step was machined in the internal channel to accommodate a 40-mesh copper wire screen placed between the vapor and liquid channels. Four additional layers of copper mesh were placed beneath the top screen to form the wicking structure. To seal the heat pipe a transparent lexan cover with a small o-ring groove was used. This lexan cover allowed the behavior of the liquid, solid, and vapor within the heat pipe to be observed visually. Heat addition ($\pm 3.4\%$) to the evaporator section was provided by a 0.58-m-long mica strip resistance heater, whereas the condenser section was cooled by a circulating fluid from a constant temperature bath through a 0.74-m coolant chamber located along the bottom of the condenser region of the heat pipe. The optimum working fluid charge was calculated to be 160 cc, whereas the actual heat pipe charge used in all tests was 170 cc. The heat pipe was slightly overcharged (6.3%) to insure full saturation of the wick. During testing, the overcharge was visually observed to be swept to the condenser region by the vapor and formed a very thin liquid layer along the top screen surface in the far condenser region. When the condenser coolant temperature was below the triple point, the excess fluid formed a thin frozen layer, and thus had no further bearing on the tests or solid blockage formation.

Instrumentation of the heat pipe included 13 stainless steel sheathed copper-constantan (T-type) thermocouples (AWG-30 and ± 0.3 K) located in the vapor channel, and 13 in the liquid channel. Beginning at 0.143 m from the leading edge of the evaporator in the liquid channel and 0.156 m in the vapor channel, the thermocouples were placed at 0.152 m intervals along the length of the heat pipe. Internal pressure measurements were provided by two Druck, Inc., model PTX 510 pressure transmitters mounted in the lexan top of the heat pipe, with one located at the end of the evaporator, P_e at 0.58 m, and one in the end region of the condenser, P_c at 1.94 m. The PTX 510 pressure transmitters were fitted with pressure sensors capable of linearly measuring absolute pressures over a full-scale range from 0 to 24.7 kPa with a 1.5% accuracy rating, including nonlinearities and hysteresis effects.

Experimental Procedure

The heat pipe was initially charged with a predetermined amount of noncondensible gas (air) to produce the desired blocked condenser length. The NCG charge is presented in terms of standard temperature and pressure (STP) conditions. The heat pipe was then brought to a steady-state condition with 160 W of evaporator power input and a condenser cooling fluid temperature of -10°C. This condition was maintained and the heat pipe was operated for a minimum of 1 h to insure steady state and to verify the noncondensible gas charge. The gas/vapor front was distinctive in nature during steady-state operation as fine condensate droplets were formed on the lexan cover in the condenser vapor region. Internal temperature measurements confirmed the location of the NCG front. This method allowed the NCG charge to be determined between 3.6 and 5.0% for the maximum to minimum NCG charges, respectively, used in this investigation. Power to the evaporator was then discontinued and the heat pipe was allowed to freeze.

Once the blockage was formed, evaporator heat addition was applied to restart the heat pipe and to melt the solid barrier. Internal temperature and pressure measurements, along with internal visual observation of the heat pipe, were conducted continuously during the restart process. For some cases, power levels below the initial 160 W were utilized during restart. In these cases the power was increased to 160 W only after the solid blockage had dissipated and only if the heat pipe was operating at a steady-state condition.

Heat Pipe Transport Capacity

To quantify the heat transport capacity of the copper/water heat pipe, the capillary limit of the heat pipe was evaluated using the methods outlined by Chi.[5] Assuming that gravitational forces are negligible, the capillary limit is given by

$$\Delta P_c \geq \Delta P_l + \Delta P_v \tag{1}$$

where ΔP_c is the maximum capillary pumping pressure, and ΔP_l and ΔP_v are the frictional losses in the liquid and vapor channels, respectively. These three terms are evaluated from the following basic equations as presented by Chi[5]

$$\Delta P_c = 2\sigma/r_c \tag{2}$$

$$\Delta P_l = \frac{(fRe)_l \mu_l}{2\varepsilon r_{h,l}^2 A_w \rho_l \lambda} q L_{\text{eff}} \tag{3}$$

$$\Delta P_v = \frac{(fRe)_v \mu_v}{2 r_{h,v}^2 A_v \rho_v \lambda} q L_{\text{eff}} \tag{4}$$

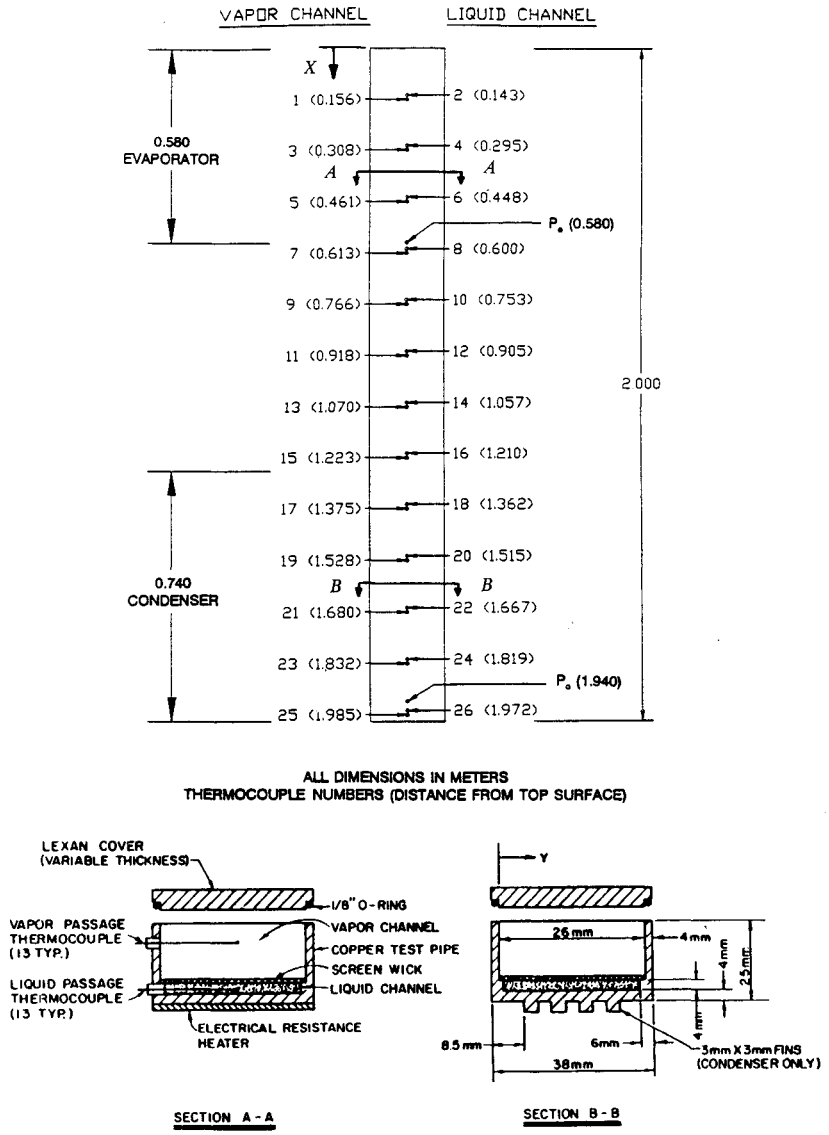

Fig. 1 Experimental test apparatus.

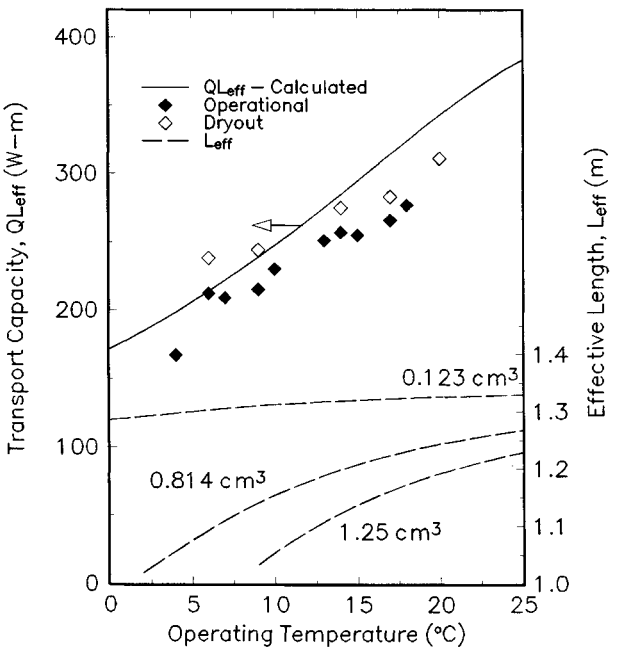

Fig. 2 Predicted heat pipe transport capacity.

The calculated transport capacity qL_{eff} is presented in Fig. 2 along with the variation in the calculated effective length L_{eff} as a function of NCG charge (volume at STP) and evaporator operating temperature T_e. The effective length L_{eff} was defined as $(L_e/2 + L_a + l_c/2)$, where l_c is the active condenser length and is based on a flat front noncondensible gas blocked region. Measured values of operating and dryout conditions for the heat pipe used in this investigation are also presented in Fig. 2, where dryout was specified to occur when a sharp rise in evaporator temperature was observed after subsequent increases in evaporator power input.

Analysis

The transient imposed on the heat pipe when the two regions regain communication may potentially result in evaporator depriming/dryout due to several mechanisms. These mechanisms include 1) mass freezeout of the fluid and depletion of the available fluid inventory, either by liquid blowby upon breakthrough or by vapor freezeout in the condenser region; or 2) exceeding the capillary pumping capability of the heat pipe during the imposed transient; or 3) vapor blockage of the liquid channel resulting from boiling or flashing in the evaporator wick—due to the rapid depressurization and assumed only possible for very large pressure differences across the blockage.

The depletion of available working fluid inventory by mass freezeout occurs in the frozen or freezing condenser regions. The amount of liquid lost during blowby is very difficult, if not almost impossible, to model and/or measure reliably, as the phenomenon is a three-dimensional, three-phase, transient condition. The amount of working fluid lost by vapor freezeout results from the variation in the vapor/gas front l_g and the melt front l_m locations, see Fig. 3. As the blockage melts, l_m progresses along the axial length of the heat pipe through the blockage. The gas front is assumed to exist directly behind the blockage on the condenser side of the vapor channel and not to vary until communication between the two sections reoccurs. However, once breakthrough occurs, the vapor/gas front is rapidly driven into the condenser region. The melt front, however, progresses at a much slower rate, thus creating a solid-vapor region between the vapor/gas front and the liquid melt front where mass freezeout m_f may occur. With sufficient time, the vapor/gas front will recede back toward the evaporator and/or the melt front will progress into the condenser region, and the two will become coincident—assuming evaporator depriming/dryout does not occur. It is important to note here that this scenario differs slightly from the conditions hypothesized in the CTS heat pipes, as noncondensible gases were presumed in the CTS case to be present on both sides of the blockage, and for the blockage to be thawed by changes in environmental conditions.

The second possible depriming mechanism, that of exceeding the capillary pumping limit of the heat pipe, results from the depressurization of the evaporator region. As the evaporator vapor pressure P_v is rapidly reduced following breakthrough, the mass flux leaving the vapor/liquid interface increases significantly, as the saturation vapor pressure P_s corresponding to the evaporator liquid temperature T_e now greatly exceeds the actual vapor pressure P_v following breakthrough. This increased mass flux results in an effective heat transport capacity q_{eff}, which exceeds the evaporator heat input rate q_e, where q_{eff} includes the superheat of the evaporator zone that must be transported to reduce the evaporator temperature to an equilibrium state with the corresponding vapor channel pressure, see Fig. 4. For the following analysis, the expansion of the vapor into the gas-blocked region is assumed to occur instantaneously (actual experiments showed that the expansion process normally occurred over a period of 10–15 s) after breakthrough as illustrated by the ideal condition in Fig. 3 and to follow an ideal gas expansion behavior.

Utilizing a control volume over the evaporator and adiabatic sections containing solid or liquid elements, an energy balance can be written as

$$\sum_{i=1}^{n} q_{e-a,i}(t) = \frac{dE_{e-a}}{dt} = (mc)_{e-a}\frac{dT_{e-a}}{dt} \tag{5}$$

where the term $(mc)_{e-a}$ is the corresponding thermal mass of the evaporator and adiabatic regions and includes the heat pipe case, heaters, wicking structure, and the liquid working fluid in the wick. The heat interaction terms $q_{e-a,i}$ include the evaporator heat input, or

$$q_{e-a,1} = q_e \tag{6}$$

and the heat released by the evaporating working fluid, or

$$q_{e-a,2} = q_{\text{eff}} = \lambda \dot{m}_v \tag{7}$$

where q_{eff} is $>q_e$ if the evaporator temperature is decreasing, $=q_e$ for steady-state conditions, or $<q_e$ if the evaporator temperature is increasing, or in the case of evaporator dryout.

As stated previously, the evaporation at an interface is extremely sensitive to variations in the vapor pressure, where an expression for the evaporation rate of an interface with only small differences between the vapor and liquid temperatures is presented as[6]

$$j_v(t) = \frac{2\alpha}{2-\alpha}\left[\frac{M}{(2\pi RT)}\right]^{0.5}(P_s - P_v) \tag{8}$$

The pressure P_s corresponds to the saturation vapor pressure at the evaporator liquid temperature T_e, which is assumed to be equal to the evaporator and adiabatic section temperature T_{e-a}. At the instant of breakthrough t_b, the vapor pressure P_v in the evaporator and adiabatic regions decreases abruptly causing the mass flux given by Eq. (8), to increase, as the evaporator liquid temperature T_e and the corresponding saturation vapor pressure P_s at this liquid temperature do not change as rapidly. The total evaporating mass flow rate is then determined by integrating Eq. (8) over the evaporating surface area

$$\dot{m}_v = \int_A j_v(t)\, dA \tag{9}$$

and is used to evaluate $q_{e-a,2}$ in Eq. (7). The time for the effective heat transport rate q_{eff} to return to an equilibrium state (assuming no dryout occurs) with the heat input rate q_e is a direct function of the mass of the heat pipe container, wick, and the working fluid liquid inventory. To evaluate the effective heat transport capacity, Eq. (5) was integrated over a specified time interval. The initial conditions of condenser pressure P_c and the evaporator temperature T_e, at the point of breakthrough t_b were specified. The accommodation coefficient α was set to 0.21.

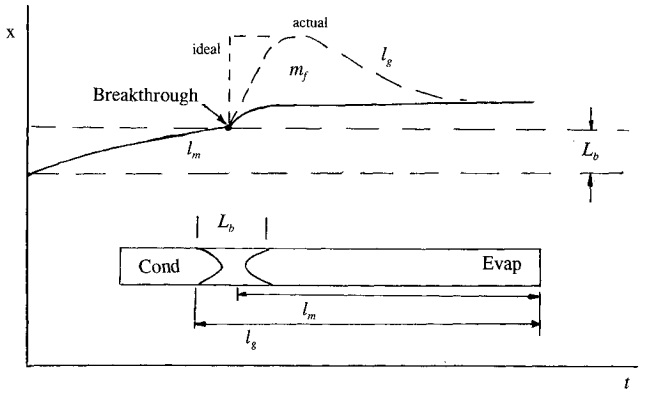

Fig. 3 Schematic of vapor/gas front and melt front behavior during restart.

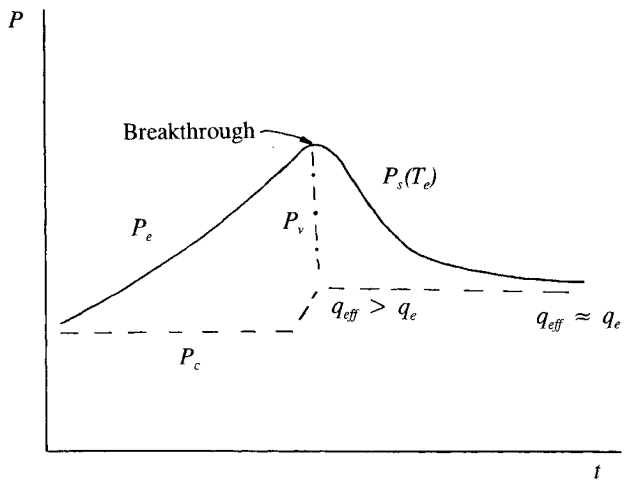

Fig. 4 Behavior of the liquid saturation vapor pressure and vapor channel pressure during the freezing blowby transient.

If the effective heat transport during the transient process is in excess of the capillary limit for the heat pipe, the dryout process of the evaporator will be initiated and result in partial dryout. In order to prevent this partial dryout condition from propagating to a total dryout, the effective heat transport capacity must not remain above the capillary limit for an extended period of time, which is dependent upon the overall thermal mass of the system, and that the liquid inventory in the heat pipe wick must be great enough to sustain any initial increases in effective heat transport levels in excess of the capillary limit.

Results

In the previous investigation of the freeze/thaw characteristics of the copper/water heat pipe, freezing blowby was present for the solid blockage corresponding to a 0.814-cm^3 gas charge of air at STP (40.5% NCG blocked condenser at 160 W).[4] As previously stated, this condition resulted in the evaporator remaining primed and the condenser and evaporator regions being decoupled by a frozen, solid blockage. The typical initial and final liquid channel temperature distributions along with the solid blockage formation contours are presented in Figs. 5 and 6, respectively, for the freezing process. The magnitude of the blockage is described by the estimated blockage volume V_b, and for this test case was estimated to be 25.0 cm^3. It is important to note here that the blockage magnitude was sensitive to changes in the NCG charge. Further tests demonstrated the characteristics of the blockage formation as a function of the NCG charge, see Fig. 7, and found that three regions with varying characteristics exist.[7] For NCG charges up to approximately 0.7 cm^3, evaporator dryout was found to occur along with the formation of a solid blockage, whereas for charges greater than approximately 1.0 cm^3, the solid blockage no longer formed, or formed incompletely, and the evaporator remained primed with liquid. The region between 0.7–1.0 cm^3 resulted in the conditions favorable to the freezing blowby phenomenon.

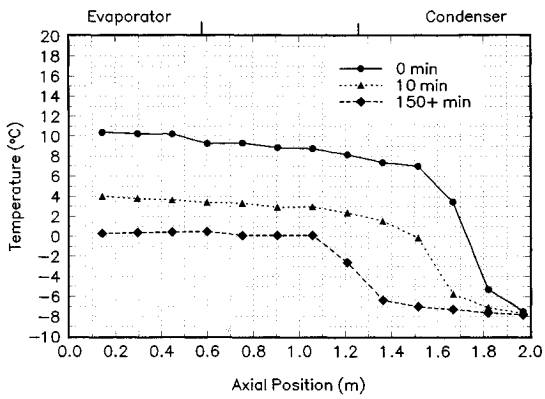

Fig. 5 Transient liquid channel temperatures during freezing for 0.814-cm^3 NCG charge.[4]

The initial restart from the configuration in Figs. 5 and 6 utilized 30 W of evaporator heat input. The corresponding transient liquid temperatures at several axial locations and the visual measurement of the solid blockage contours are presented in Figs. 8 and 9, respectively, for an estimated V_b of 25.0 cm^3, with the thermocouple numbers presented in Fig. 8 corresponding to the thermocouples and locations outlined in Fig. 1. No pressure measurements were available for this restart case.[4] As shown, the temperatures in the evaporator region decreased immediately following breakthrough of the blockage, due to the corresponding decrease in vapor pressure as the high-pressure evaporator region vented into the previously decoupled condenser region. However, depriming of the liquid channel was not observed for this restart condition, and as shown, the heat pipe was returned to an operating state with a power input of 160 W. Visually, liquid was observed to be propelled into the condenser region by the vapor to a distance of approximately 6.0 cm from the condenser end of the blockage. However, the liquid driven into the condenser was limited to liquid supplied from the melting blockage. After breakthrough, it was impossible to determine with any accuracy the percentage of liquid that resulted from the solid blockage that was frozen out in the condenser, and the percentage that re-entered the wicking structure.

Further analysis of restart with low evaporator heat inputs (30 W) and internal pressure measurements resulted in similar observations and the ability to return the heat pipe to the previous operating condition. The transient liquid channel temperatures and vapor channel pressures for a blockage volume of 20.9 cm^3 resulting from a NCG charge of 0.995 cm^3 are presented in Fig. 10. From the pressure measurements, it was apparent that no communication between the two regions was present prior to melting of the barrier. The most noticeable difference between the results occurring for a

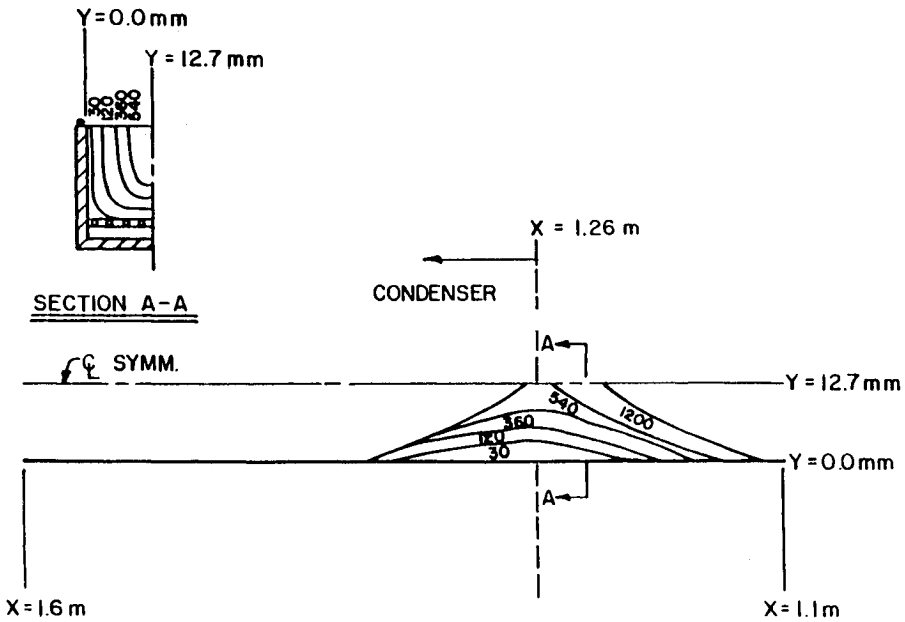

Fig. 6 Solid formation contours for 0.814-cm^3 NCG charge during freezing.[4]

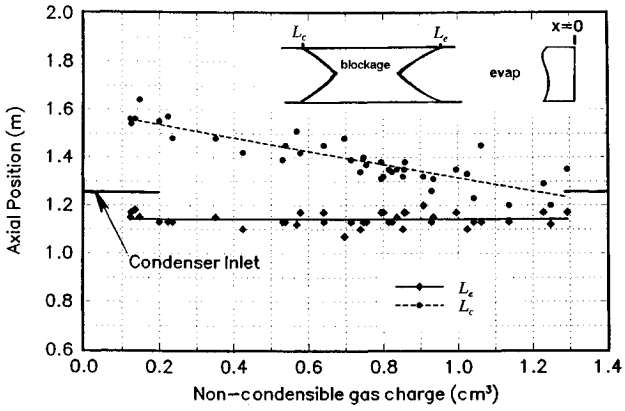

Fig. 7 Effect of noncondensible gas charge on vapor channel blockage.

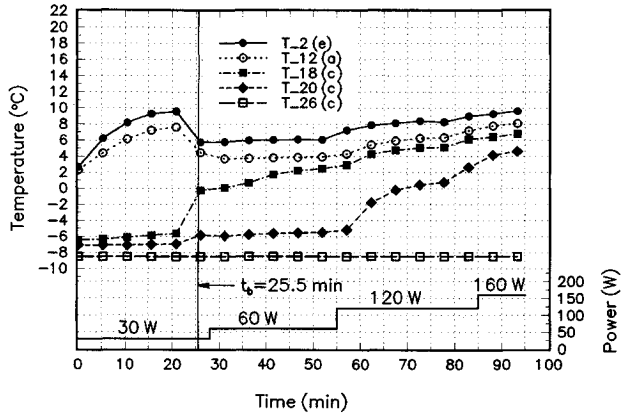

Fig. 8 Transient liquid channel temperatures for restart with V_b = 25.0 cm³ and 0.814-cm³ NCG charge.[4]

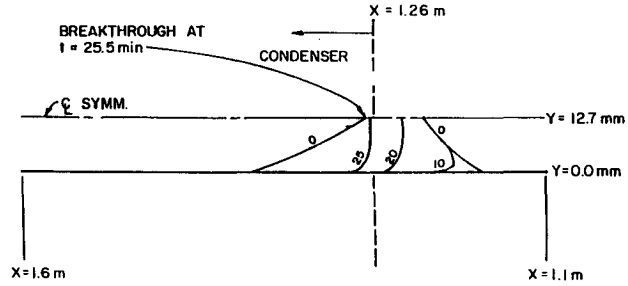

Fig. 9 Solid blockage contours during restart with V_b = 25.0 cm³ and 0.814-cm³ NCG charge.[4]

blockage volume of 25.0 cm³ and 20.9 cm³ was the time required for breakthrough of the barrier, 25.5 min vs 15.0 min. This is indicative of the overall heat necessary to melt the blockage, and as the time required for breakthrough decreased, the magnitude of the evaporator temperatures was also found to decrease. Also presented in Fig. 10, are the calculated effective heat transport capacity and capillary limit. As seen, q_{eff} easily exceeds the capillary limit by a factor of 3 in this case, even for a very low pressure differential across the blockage (≈200 kPa). However, q_{eff} rapidly decreased below the capillary limit and the heat pipe was able to operate without dryout occurring.

Results of restart for a high-power input level of 200 W are presented in Fig. 11 for a NCG charge of 0.800 cm³ and corresponding blockage volume of 30.9 cm³. This increased heat input rate significantly reduced the time required for melting of the solid blockage, however, it also increased the

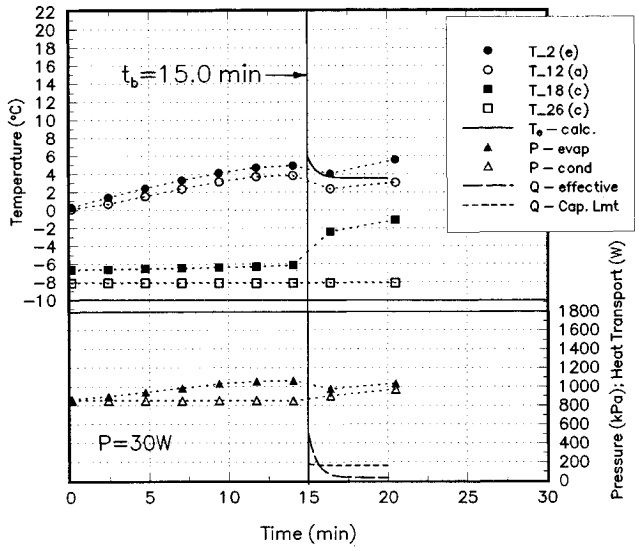

Fig. 10 Restart for V_b = 20.9 cm³ and 0.995-cm³ NCG charge.

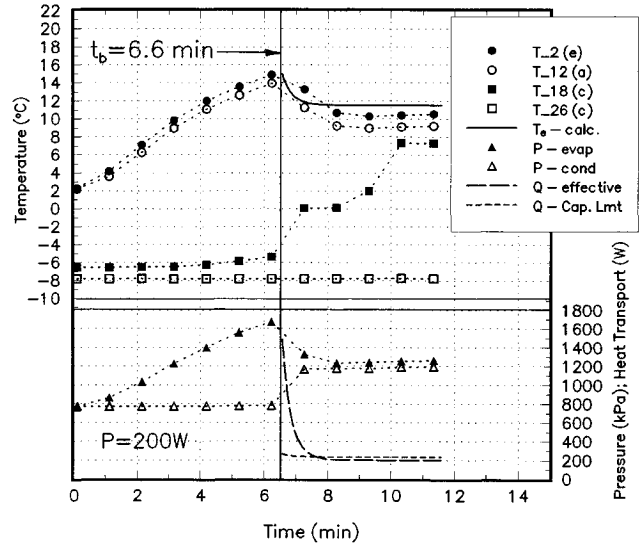

Fig. 11 Restart for V_b = 30.9 cm³ and 0.800-cm³ NCG charge.

evaporator pressure and temperature prior to breakthrough. Visually, the liquid in the case of an increased heat addition rate resulted in the liquid being propelled by as much as 12.0 cm past the condenser end of the blockage. Again, this liquid appeared to be limited to liquid supplied by the melting blockage only. Evaluation of q_{eff} also demonstrated a marked increase in the effective heat transport rate during the depressurization process. The heat pipe for this test was again returned to a steady-state operating condition. It is important to note that the calculated evaporator temperature decreased at a noticeably greater rate than the measured liquid temperatures. This is presumed to result from the assumption of an instantaneous expansion of the high-pressure evaporator region into the condenser region. Correspondingly, the initial calculated q_{eff} will be slightly exaggerated, however, the time required for q_{eff} to fall below the capillary limit will be increased, as the overall quantity of heat carried out of the evaporator region must be the same in both cases.

A restart with 160 W of evaporator heat addition is presented in Fig. 12 for an NCG charge of 0.754 cm³ and a much greater blockage volume of 36.4 cm³, with internal liquid channel temperatures only because the pressure transducers had not yet been installed. In this situation, evaporator dryout, marked by the sharp rise in evaporator temperature, was

Table 1 Summary of experimental results

NCG, cm³	V_b, cm³	Power, W	ΔP_{max}, Pa	$T_{e,max}$, °C	t_b, min	Dryout
0.738	35.2	30	N/A	6.8	28.5	No
0.747	38.2	160	600	15.0	8.0	No
0.754	36.4	160	N/A	17.3	10.5	Yes
0.794	19.5	160	620	14.3	7.6	No
0.800	30.9	200	601	15.2	6.6	No
0.814	25.0	30	N/A	9.6	25.5	No
0.823	26.4	160	380	9.5	4.7	No
0.836	22.8	160	1300	21.0	11.4	No
0.852	23.7	80	N/A	6.8	8.0	No
0.995	20.9	30	200	5.3	15.0	No

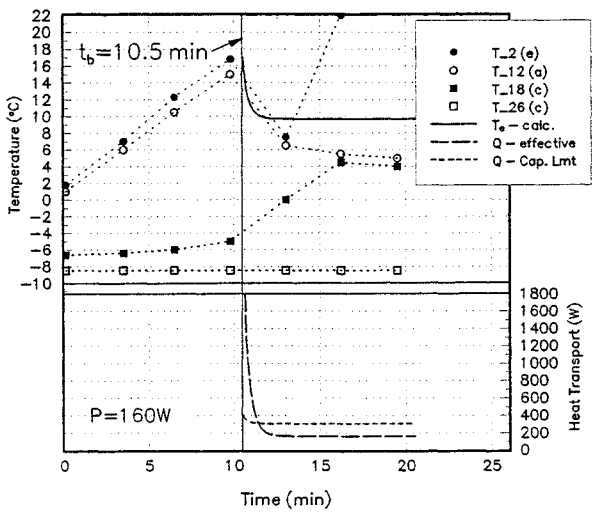

Fig. 12 Restart for V_b = 36.4 cm³ and 0.754-cm³ NCG charge.

observed to occur following breakthrough of the barrier. As the evaporator temperature prior to breakthrough was greatly elevated, q_{eff} after breakthrough easily exceeded the capillary limit by an order of magnitude.

Discussion of Results

The experimental results presented in the above section along with several other restart tests in this investigation are summarized in Table 1. These include the following values prior to breakthrough: the maximum pressure difference across the blockage ΔP_{max}, the maximum evaporator liquid channel temperature $T_{e,max}$, and the time required for breakthrough t_b. As seen from these results, only one case resulted in evaporator dryout, that of a blockage volume of 36.4 cm³ and an input evaporator power of 160 W. Intuitively, this could be attributed to the larger temperature drop, and correspondingly, the greater pressure gradient driving the working fluid farther into the condenser region. However, the cause of the evaporator dryout in this case may also be attributed to the magnitude of the blockage formation itself. The working fluid that froze to create the increased blockage must have been supplied from the evaporator wick, thus reducing the available working fluid, or the level of saturation in the wicking structure. Because this blockage formation was the greatest in magnitude, the level of desaturation in the evaporator would be assumed to be the greatest as well. Upon breakthrough of the blockage, the rapid decrease in pressure resulted in an instantaneously increased vaporization rate, represented by q_{eff}, in the evaporator and imposed a transient on the heat pipe liquid channel too great for the depleted wicking structure to accommodate. This increased evaporation rate is seen to be more significant in heat pipe dryout as the actual mechanism of liquid being blown into the condenser region.

The heat pipe utilized in the current investigation was believed to not dry out for the vast majority of tests due to the availability of sufficient working fluid in the wicking structure to sustain the imposed depressurization transient. As stated earlier, the single dryout was believed to result from the inadequate supply of working fluid in the wicking structure and highlights the above requirements for the heat pipe to sustain the imposed transient. Also, the fluid melted from the blockage during initial thawing (i.e., prior to breakthrough) was visually observed to rewet the adjacent wicking structure slowly due to the combination of the governing fluid properties near the triple point (i.e., liquid viscosity, surface tension, and wetting angle) being elevated, and therefore, least favorable for wetting of the wick.

The liquid feed to the wicking structure is dependent on the advancement of the melt front in the condenser section. As discussed earlier, the vapor that penetrates the blockage rapidly progresses into the vapor channel of the condenser while the melt front takes several minutes to progress the same distance. Thus, the liquid feed rate is dependent on the time required to melt the fluid in the condenser region and may lag behind the fluid transport rate to the condenser. It is important here to note the differences when the heat pipe with larger levels of NCG (>1.1 cm³), such that no blockage formed, were tested.[4,7] The liquid melt front and the vapor front in this case proceed at essentially the same rate into the condenser during restart. Thus, without the blockage, the coincident melt front and NCG front rates are the controlling factor in the restart characteristics of the heat pipe.

In contrast to the current investigation, the VCHPs used onboard the CTS were assumed to be operating prior to breakthrough of the solid barrier, as the barrier was only deemed to melt when the environmental temperature was increased. Also, noncondensible gases could be present on both sides of the blockage—unlike the conditions found in this investigation. If the heat pipe is operating prior to breakthrough, the wick in the evaporator may not be fully saturated and thus, the liquid inventory may not be able to sustain the imposed transient. Also, the liquid that is blown into the condenser would inevitably only result from the melted blockage, which was formed from the excess charge. Any transport of fluid from the evaporator to the condenser, where it may or may not freeze, would be in the form of vapor freezeout (assuming that the increased vapor velocities do not induce entrainment). Thus, the transient inflicted by the depressurization of the evaporator may be as great, if not greater, a mechanism resulting in evaporator depriming.

For industrial applications of heat pipes, two additional problems could exist. First, the heat pipes are typically attached to a thermal mass of much greater thermal capacity than the heat pipe itself, thus, the effective heat transport capacity would remain above the capillary limit for a significantly increased amount of time and more easily induce dryout. If dryout occurs, the effective heat transport must decrease below the capillary limit based on the open artery or axial

pumping capability of the wicking structure for rewetting to occur. Secondly, the temperature measurements for the given heat pipe were not sensitive enough to determine the magnitude of the solid blockage formation. Only visual data through the use of the lexan cover could provide this information.

Conclusions

The phenomenon of freezing blowby was investigated for various rates of restart and magnitudes of vapor channel blockage. Restart was accomplished in all cases except one, which was believed to result directly from the reduced liquid inventory in the wicking structure prior to restart. Upon breakthrough of the blockage, the depressurization results in an increased evaporation rate at the liquid surface in the evaporator and may cause evaporation in the adiabatic region as well. This increased evaporation rate corresponds to an effective heat transport capacity in excess of the existing evaporator power input. The transient imposed on the heat pipe by the effective heat transport capacity can be more severe than the loss of liquid blown into the condenser section after breakthrough, and may be a more significant parameter in the potential failure of the heat pipe, since for this case the traditional capillary limitation of the heat pipe must be able to sustain the increase. The analysis demonstrated that the effective heat transport capacity can easily exceed the capillary pumping limit by an order of magnitude.

Acknowledgment

The authors would like to acknowledge the support of the NASA Office of Commercial Programs (Code C) through the Texas A&M University Center for Space Power, College Station, Texas.

References

[1]Antoniuk, D., and Edwards, D. K., "Depriming of Arterial Heat Pipes: An Investigation of CTS Thermal Excursions," NASA Lewis Research Center, NASA CR 165153, Cleveland, OH, Aug. 1980.

[2]Antoniuk, D., and Edwards, D. K., "Depriming of Arterial Gas-Controlled Heat Pipes," *Proceedings of the 7th International Heat Pipe Conference* (Minsk, USSR), 1990.

[3]Antoniuk, D., "Generalized Modeling of Steady State and Transient Behavior of Variable Conductance Heat Pipes," AIAA Paper 87-1615, June 1987.

[4]Ochterbeck, J. M., and Peterson, G. P., "Visualization of the Freeze/Thaw Characteristics of a Copper/Water Heat Pipe: Effects of Non-Condensible Gas Charge," *Journal of Thermophysics and Heat Transfer*, Vol. 7, No. 1, 1993, pp. 127–132.

[5]Chi, S. W., *Heat Pipe Theory and Practice*, Hemisphere, Washington, DC, 1976.

[6]Collier, J. C., *Convective Boiling and Condensation*, McGraw-Hill, New York, 1981, pp. 316–318.

[7]Ochterbeck, J. M., "Freeze/Thaw Characteristics of Room Temperature Heat Pipes—Incorporating Thermal History Effects and Non-Condensible Gas Charging," Ph.D. Dissertation, Texas A&M Univ., College Station, TX, Aug. 1993.